Planetary and Space Science ∎ (∎∎∎∎) ∎∎∎–∎∎∎

Contents lists available at ScienceDirect

Planetary and Space Science

journal homepage: www.elsevier.com/locate/pss

Constraints on the abundance of carbon in near-surface materials on Mercury: Results from the MESSENGER Gamma-Ray Spectrometer

Patrick N. Peplowski [a,*], David J. Lawrence [a], Larry G. Evans [b], Rachel L. Klima [a], David T. Blewett [a], John O. Goldsten [a], Scott L. Murchie [a], Timothy J. McCoy [c], Larry R. Nittler [d], Sean C. Solomon [d,e], Richard D. Starr [f], Shoshana Z. Weider [d]

[a] The Johns Hopkins University Applied Physics Laboratory, Laurel, MD 20723, USA
[b] Computer Science Corporation, Lanham-Seabrook, MD 20706, USA
[c] National Museum of Natural History, Smithsonian Institution, Washington, DC 20013, USA
[d] Department of Terrestrial Magnetism, Carnegie Institution of Washington, Washington, DC 20015, USA
[e] Lamont-Doherty Earth Observatory, Columbia University, Palisades, NY 10964, USA
[f] Department of Physics, Catholic University of America, Washington, DC 20064, USA

ARTICLE INFO

Article history:
Received 27 August 2014
Received in revised form
14 January 2015
Accepted 19 January 2015

Keywords:
Mercury
Gamma-ray spectroscopy
Geochemistry

ABSTRACT

Mercury's low surface reflectance and the low surface abundances of iron and titanium have led to the suggestion that carbon (C) may serve as the dominant darkening agent on Mercury's surface. Estimates of the amount of carbon required to achieve the observed surface darkening are within the sensitivity range of measurements by MESSENGER's Gamma-Ray Spectrometer (GRS). We use GRS measurements to constrain the C content of Mercury's surface, the first such use of gamma-ray spectroscopy data. Our methodology includes techniques for removing background contributions to the measured signal and is broadly applicable to any gamma-ray spectroscopy dataset. The measured C content for Mercury's surface, 1.4 ± 0.9 wt%, is consistent with 0–4.1 wt% C at the three-standard-deviation level and therefore does not represent a definitive detection of C at the surface. Possible mechanisms for providing up to 4.1 wt% C on Mercury's surface include primordial and exogenous sources. Additional measurements at low altitude made with MESSENGER's Neutron Spectrometer can yield further constraints on the C content of Mercury's surface.

1. Introduction

An important feature of Mercury's surface is its globally low reflectance compared with that for the Moon (Robinson et al., 2008, and references therein). Since the reflectance of airless silicate bodies is a function of surface composition and soil maturity, differences in average reflectance between the Moon and Mercury suggest that there are important differences in their surface characteristics. Soil maturation occurs as a result of space weathering, and the set of processes by which space weathering occurs are expected to mature surface materials on Mercury faster than on the Moon (e.g., Noble and Pieters, 2003). However, examination of comparably immature regions on the Moon and Mercury reveal differences in reflectance that are likely primarily due to differences in the surface compositions of these two bodies (Braden and Robinson, 2013). Investigations of Mercury's surface composition by the MErcury Surface, Space ENvironment, GEochemistry, and Ranging (MESSENGER) spacecraft, which was inserted into orbit about Mercury on 18 March 2011, have confirmed substantial differences in major-element composition between the surfaces of Mercury and the Moon (Nittler et al., 2011; Weider et al., 2012; Evans et al., 2012). In particular, Mercury has higher Mg/Si and S/Si but lower Al/Si, Ca/Si, and Fe/Si ratios by weight than lunar surface material. More generally, Mercury lacks both the Fe-rich basalts found in the lunar maria as well as the plagioclase-dominated material found in the lunar highlands. Mercury's surface appears instead to be dominated by Fe-poor basalts that consist of Mg-rich orthopyroxene and plagioclase (Stockstill-Cahill et al., 2012).

Under the assumption that surface composition exerts a primary control on Mercury's average reflectance, a number of opaque darkening agents have been proposed. They include Fe–Ti oxides such as ilmenite ($FeTiO_3$; Denevi et al., 2009), submicroscopic metallic iron (Lucey and Riner, 2011), and high-Ti cumulates formed during crystallization of an early magma ocean (Riner et al., 2009). These materials would be expected to be particularly abundant in Mercury's low-reflectance material (LRM), which have reflectance values as much as 30% below the global mean (Robinson et al., 2008; Denevi et al., 2009). Fig. 1 shows an example of an LRM

* Corresponding author.
E-mail address: Patrick.Peplowski@jhuapl.edu (P.N. Peplowski).

http://dx.doi.org/10.1016/j.pss.2015.01.008
0032-0633/

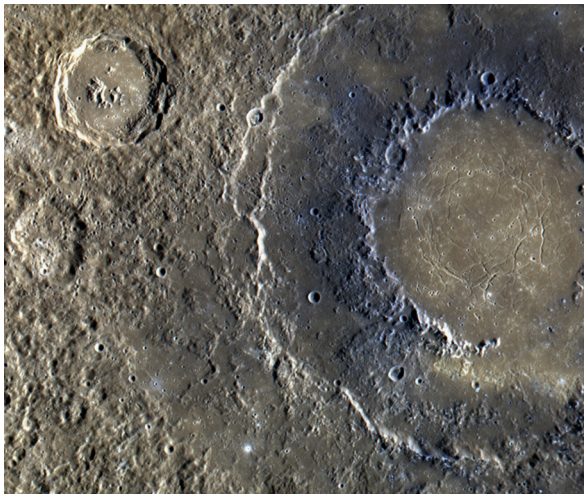

Fig. 1. MESSENGER Mercury Dual Imaging System (MDIS) color-composite image of a portion of the 290-km-diameter Rachmaninoff impact basin. This image was created by using three images acquired as part of MESSENGER's color base map at central wavelengths of 1000, 750, and 430 nm and displaying them in red, green, and blue, respectively. The dark blue material near the inner ring of the basin is an example of low-reflectance material (LRM), the reflectance of which is attributed to the addition of a darkening agent to material otherwise similar to surface material elsewhere on the planet. Created from MDIS wide-angle camera images 1261261, 1261260, and 1261259.

deposit located within the Rachmaninoff impact basin (Prockter et al., 2010). This deposit represents one of the largest LRM features in the northern hemisphere and highlights the observation that the LRM frequently appears as excavated material and may be a common component of the mid to lower crust (Denevi et al., 2009; Ernst et al., 2010).

Hypotheses that invoke large abundances of Fe and Ti in darkening agents have proven to be inconsistent with the measurements of elemental composition of Mercury's surface material returned by the MESSENGER X-Ray Spectrometer (XRS) (Schlemm et al., 2007) and Gamma-Ray Spectrometer (GRS) (Goldsten et al., 2007). XRS and GRS data indicate that the surface of Mercury is low in both Fe (1–4 wt% global; 1.9 ± 0.3 wt% northern hemisphere average) and Ti (≤ 0.8 wt% global) (Nittler et al., 2011; Evans et al., 2012; Weider et al., 2014). XRS measurements within the LRM indicate Ti abundances of < 1 wt% (Murchie et al., 2015), demonstrating that there is no appreciable increase in Ti content within these regions. These observations are inconsistent with the presence of sufficient amounts of ilmenite, submicroscopic metallic Fe, or Ti to account for Mercury's low reflectance overall and for the differences in reflectance observed among major spectral units. Moreover, spatially resolved measurements of Fe show no correlation with reflectance or the slope of the reflectance spectrum (Weider et al., 2014), further indicating that iron or Fe-rich compounds cannot be the dominant darkening agent on Mercury.

Carbon has also been proposed as a possible darkening agent on Mercury (Blewett et al., 2009; Denevi et al., 2009; Bruck Syal et al., 2013; Murchie et al., 2015). As little at 1 wt% C in the form of fine-grained graphite can account for Mercury's globally averaged reflectance, and ~5 wt% C could lower the reflectance to that of LRM (Murchie et al., 2015). These C abundances are markedly larger than the crustal abundances found on Earth, Mars, or the Moon (Lodders and Fegley, 1998), where C is a trace element for which the typical abundance is ≤ 1000 ppm. No current theory of planet formation or evolution predicts that Mercury's surface should have ≥ 1 wt% C on an average. Nonetheless, Mercury's surface composition is sufficiently distinct from those of the other terrestrial planets that the geochemical properties of those bodies need not limit consideration of scenarios for the innermost planet.

At sufficiently high concentrations (~0.5 wt% or higher), carbon is within the detectability range of gamma-ray spectroscopy measurements. For the MESSENGER GRS data, the analysis required to detect C is complicated by the presence of large, spacecraft-originating backgrounds. We combine gamma-ray production and transport modeling with an analysis of the GRS carbon signature and spectral background reduction techniques to constrain the abundance of C on Mercury's surface. We discuss the implications for this result, including possible primordial and exogenous sources, as well as potential follow-up investigations with MESSENGER's Neutron Spectrometer (NS).

2. Gamma-ray spectroscopy

2.1. Planetary gamma-ray production

Planetary gamma-ray spectroscopy involves measurement of the spectrum of gamma rays emitted from a planetary surface to derive information on surface composition. Gamma rays are produced by the interaction of high-energy galactic cosmic ray (GCR) protons with atomic nuclei in near-surface planetary material. The GCRs produce neutrons in the uppermost ~2 m of regolith via spallation reactions, and those neutrons can excite individual nuclei to unstable states. These excited nuclei frequently decay back to their ground states via the emission of gamma rays at element-characteristic energies. Measurements of these gamma rays are therefore diagnostic of planetary surface composition. Deriving elemental abundances from gamma-ray measurements requires knowledge of the detector response, gamma-ray background signals, and gamma-ray production cross sections. Orbital gamma-ray spectroscopy has been successfully applied to study the composition of the Moon (e.g., Prettyman et al., 2006), Mars (Boynton et al., 2007), Mercury (e.g., Evans et al., 2012), and asteroid 4 Vesta (e.g., Prettyman et al., 2012). The elements H, O, Na, Mg, Al, Si, S, Cl, K, Ca, Ti, Fe, Th, and U have all been measured to date with orbital gamma-ray measurements.

Gamma-ray spectroscopy is insensitive to surface properties (e.g., grain size, roughness) and viewing geometry (e.g., incidence and emission angles), and it samples surface composition to depths of tens of centimeters. Drawbacks of gamma-ray spectroscopy include the broad spatial resolution of the measurements, approximately a factor of 1.5 greater than the orbital altitude, and long measurement times needed because of low counting rates. The latter necessitates making measurements in close proximity to a planetary surface (i.e., at altitudes $\leq$ the radius of the target body). During MESSENGER's primary mission (18 March 2011–17 March 2012) the spacecraft was in a 12-h-long, highly eccentric orbit. Only ~45 min of each orbit were at sufficiently low altitudes (< 2000 km) to characterize the surface gamma-ray flux with statistical significance. This portion of the orbit, because of the high northern periapsis, was restricted to the northern hemisphere of Mercury. As a result of this limitation, the abundances of many elements have been reported only as northern hemisphere averages (Evans et al., 2012).

2.2. Carbon gamma-ray signature

Carbon is a stable element that is found predominantly (98.93%) in the form of ^{12}C. When the ^{12}C nucleus is excited by a high-energy ($E_n > 4.4$ MeV) neutron, it temporarily occupies a higher-energy state before returning to its stable ground state by emitting element-characteristic gamma rays. This process, called neutron inelastic scattering, is denoted as

$$^{12}C + n \rightarrow {}^{12}C + n' + \gamma$$

Please cite this article as: Peplowski, P.N., et al., Constraints on the abundance of carbon in near-surface materials on Mercury: Results from the MESSENGER Gamma-Ray Spectrometer. Planetary and Space Science (2015), http://dx.doi.org/10.1016/j.pss.2015.01.008

or alternatively as $^{12}C(n,n'\gamma)^{12}C$. Here n represents the incident neutron, n′ represents the now lower-energy neutron following the inelastic scatter, and γ is a gamma ray. A 4438-keV gamma ray is typically emitted during this reaction and is hereafter denoted as γ_{4438}. This reaction has a high probability (cross section) to occur; thus the C signal is potentially detectable even for low ($\geq \sim 0.5$ wt%) abundances of carbon. The precise sensitivity depends on the details of the gamma-ray spectrometer and measurement parameters such as altitude and accumulation time.

The 4438-keV gamma ray is emitted while the ^{12}C nucleus is still recoiling from the neutron interaction. As a result, the emission line is Doppler broadened to a full-width half-maximum (FWHM) of ~80 keV. This FWHM is much wider than the intrinsic energy resolution of the MESSENGER GRS (FWHM ~4.5 keV at 1332 keV). Although this Doppler broadening is not unique to ^{12}C, the vast majority of gamma decays occur after the nucleus has stopped recoiling and are therefore not Doppler broadened. Analysis of the 4438-keV peak must accommodate the fact that it is wider than the majority of peaks of interest, and its width reduces the signal-to-background of the C signature relative to non-broadened peaks.

No previous planetary gamma-ray spectroscopy experiment has reported a C abundance, although a C signature was observed in the Mars Odyssey GRS measurements (Evans et al., 2006). That signature originated primarily from CO_2 in the martian atmosphere and polar caps and was not analyzed in detail. This analysis is the first attempt to derive a C abundance for a planetary surface from gamma-ray measurements.

2.3. Carbon gamma-ray backgrounds

Spacecraft-originating 4438-keV background signals are a major complication in the analysis of the C gamma-ray signature. These backgrounds are produced by GCR-induced gamma-ray production within MESSENGER's carbon-composite structure and carbon-fiber sunshade, and within the GRS anti-coincidence shield, an organic scintillator that surrounds the gamma-ray sensor. This background must be removed from the GRS measurements in order to determine the fraction of the 4438-keV gamma-ray count rate that originates from the surface of Mercury. A major benefit to MESSENGER's highly eccentric orbit about Mercury is that the GCR-induced background is sampled during every orbit, as the highest altitudes (8000 to 16,500 km) are beyond the altitude range at which there is a notable signal from Mercury (< 5000 km).

2.4. Interfering signal from oxygen

There is an additional source of background for the 4438-keV C peak that originates from neutron-induced reactions on ^{16}O. These reactions convert ^{16}O to ^{12}C as

$$^{16}O + n \rightarrow {}^{12}C + n' + \alpha + \gamma_{4438}$$

and emit a 4438-keV gamma ray in the process. The symbol α denotes that an alpha particle is emitted during this reaction. This process occurs on both the spacecraft and on planetary surfaces. During our analysis, we do not segregate C- and O-originating spacecraft backgrounds, and they are therefore removed from the measured 4438-keV signal together. In contrast, the surface components are treated individually in order to separate the O and C signals and derive a C abundance.

Although the probability for the above reaction to occur is low, the abundance of O is expected to be an order of magnitude (or more) higher than that of C on Mercury on the basis of C/O abundance ratios of other inner solar system materials (Lodders and Fegley, 1998). Using knowledge of the gamma-ray production cross sections for the

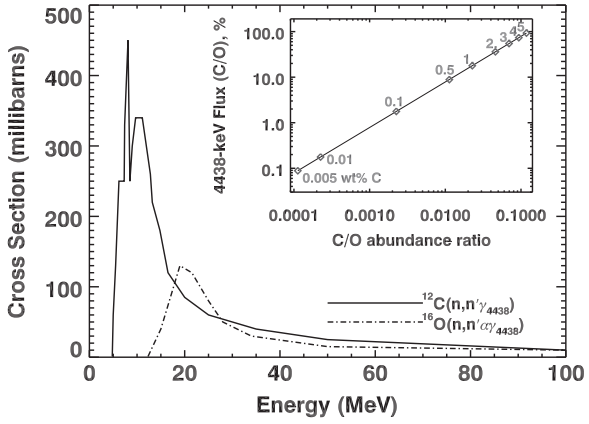

Fig. 2. Gamma-ray production cross sections for 4438-keV emission from ^{12}C (solid line) and ^{16}O (dashed line). The inset shows the fraction of the 4438-keV surface flux that originates from C as a function of the C/O abundance ratio (by weight) of surface material.

$^{12}C(n,n'\gamma)$ and $^{16}O(n,n'\alpha\gamma)$ reactions (Fig. 2), we applied the formalism presented in the appendix to calculate the fraction of the 4438-keV count rate originating from C as a function of the C/O abundance ratio. Eq. (A7) provides this value as a function of the atomic ratios for these two elements, and the ratio is plotted as a function of the mass ratio in Fig. 2 (inset). The figure reveals that for C abundances greater than 0.5 wt%, C contributes 10% or more to the measured count rate. For abundances greater than 3 wt%, C dominates 4438-keV gamma-ray production.

We checked the validity of our gamma-ray production calculations (Fig. 2) using the radiation transport code MCNPX (Pelowitz, 2005). MCNPX has a long history of application to planetary gamma-ray spectroscopy (e.g., Prettyman et al., 2006; Boynton et al., 2007; Evans et al., 2012). GCR-induced gamma-ray production was modeled for 40 planetary material compositions, including lunar samples and meteorites. The modeled flux of 4438-keV gamma rays is plotted versus O abundance in Fig. 3a. The data generally follow a trend of increasing flux with increasing O abundance. A linear relationship was derived using the lowest C abundance samples, and the differences between this fit and the simulated 4438-keV gamma-ray flux are plotted for each point as a function of C content in Fig. 3b. A clear trend of higher O-detrended 4438-keV gamma-ray count rates as a function of increasing C content is observed, further demonstrating that C is detectable via gamma-ray spectroscopy for concentrations of ~1 wt% or greater.

The absolute contribution from O to the 4438-keV count rate can be calculated by scaling the measured 6129-keV gamma-ray count rate by the ratio of the cross sections for 4438- to 6129-keV gamma-ray production from ^{16}O (0.26, Eq. (A9)) multiplied by the relative detection efficiency of the GRS at these energies (1.6; Eq. (A10)). We note that the 6129-keV gamma ray originates primarily from neutron inelastic scattering on ^{16}O, but that it also includes a minor (0.1) contribution from the

$$^{16}O + n \rightarrow {}^{16}N + p$$

reaction that must be removed, as ^{16}N subsequently decays to ^{16}O, a process that is frequently (67%) accompanied by a 6129-keV gamma ray. The symbol p denotes that a proton is emitted during this reaction.

3. Measured gamma-ray signal

3.1. Peak analysis

The analysis for this study used anti-coincidence gamma-ray spectra acquired by the MESSENGER GRS. The spectra are classified

Please cite this article as: Peplowski, P.N., et al., Constraints on the abundance of carbon in near-surface materials on Mercury: Results from the MESSENGER Gamma-Ray Spectrometer. Planetary and Space Science (2015), http://dx.doi.org/10.1016/j.pss.2015.01.008

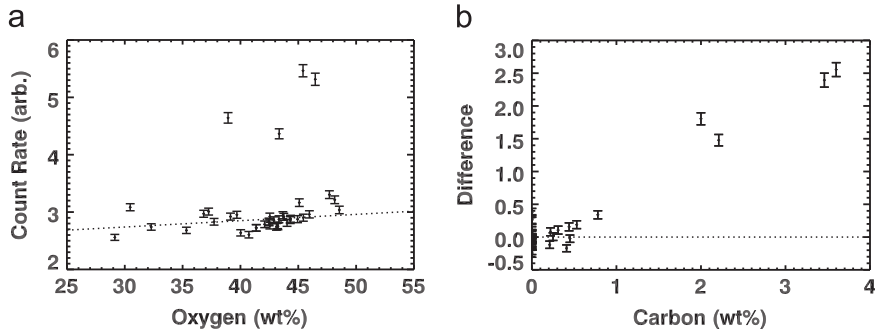

Fig. 3. (a) MCNPX-modeled 4438-keV gamma-ray flux (in arbitrary units) as a function of O content for 40 lunar and meteorite samples. (b) Difference between the modeled 4438-keV count rates and those derived from a linear relationship fit with only the low-C samples, plotted as a function of C content. The trend of increasing differences with increasing C content demonstrates the sensitivity of gamma-ray measurements to C for abundances >1 wt%.

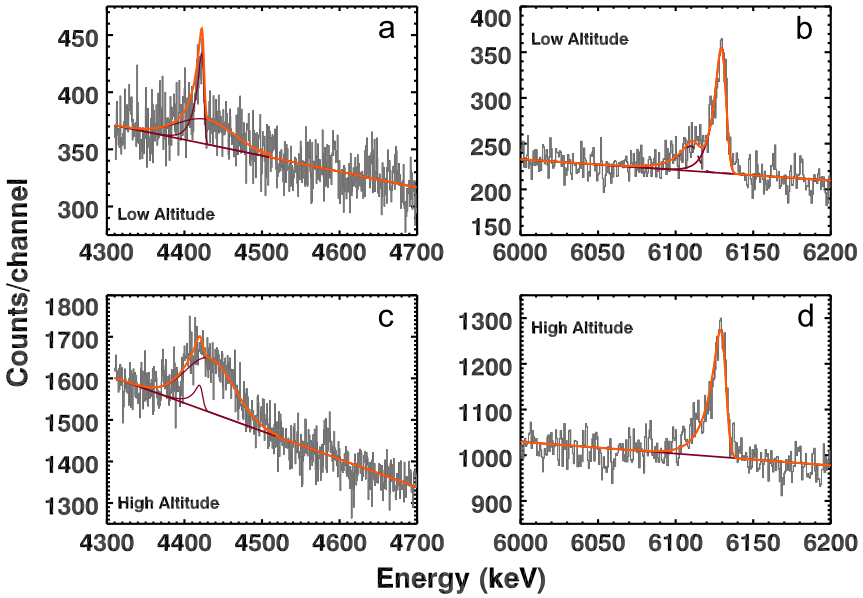

Fig. 4. Spectral peak fitting for the high-altitude (HA; >8000 km) and low-altitude (LA; <2000 km) gamma-ray measurements. The energy regions of interest from top to bottom and left to right are (a) LA 4438-keV, (b) LA 6129-keV, (c) HA 4438-keV, and (d) HA 6129-keV regions. The red lines detail the individual background and peak fits, and the orange lines show the full fits. The peak-area-derived count rates for these fits are given in Table 1. Similar peak fits were utilized to derive Si and Ti peak areas; details of those fits are provided by Peplowski et al. (2012).

and summed by orbital altitude at acquisition, with the high-altitude spectrum equal to the sum of all GRS data acquired at altitudes above 8000 km and the low-altitude spectrum equal to the sum of all data acquired at altitudes below 2000 km. Evans et al. (2012) showed that a 2000 km cutoff for the low-altitude spectrum maximized the statistical significance of most gamma-ray measurements. The high-altitude spectrum has been used to characterize the GCR-induced background, and the low-altitude spectrum has been used to characterize the signal from Mercury. Each sum was compiled from data acquired during optimal measurement times (e.g., no interfering solar activity, good high-voltage levels on the detector), and the low-altitude data were restricted to nadir-viewing geometries in order to limit variability induced by the incident-angle-dependent response of the GRS (Peplowski et al., 2012). Both sums were compiled from measurements taken between 24 March 2011 and 28 September 2011, the time period during which the GRS was operating with its optimal energy resolution.

Peak fits were performed on the spectra to derive peak areas for the 4438-keV C, 6129-keV O, 1779-keV Si, and 983-keV Ti gamma-ray signatures (Fig. 4). The peak areas were corrected for the live-time-corrected accumulation time and energy bin width to derive the gamma-ray count rate at the detector. The details of the spectral analysis procedure can be found in Peplowski et al. (2011, Supplementary online material). The results of the spectral analysis for each of the four peaks of interest are listed in Table 1.

Table 1
Gamma-ray count rates derived from spectral fitting of summed low- (<2000 km) and high- (>8000 km) altitude spectra. Units are counts per min (cpm).

		Count rates			
		High-altitude		Low-altitude	
Element	Energy (keV)	Count rate (cpm)	Error (cpm)	Count rate (cpm)	Error (cpm)
Carbon	4438	0.143	0.005	0.340	0.025
Oxygen	6129	0.056	0.002	0.329	0.020
Silicon	1779	0.241	0.006	2.574	0.043
Titanium[a]	983	0.518	0.018	0.774	0.047

[a] From Peplowski et al. (2012).

The inclusion of the Si peak analysis follows from previous MESSENGER GRS analyses (Evans et al., 2012; Peplowski et al., 2014), where stable-element abundances are presented as weight

Please cite this article as: Peplowski, P.N., et al., Constraints on the abundance of carbon in near-surface materials on Mercury: Results from the MESSENGER Gamma-Ray Spectrometer. Planetary and Space Science (2015), http://dx.doi.org/10.1016/j.pss.2015.01.008

ratios to Si in order to remove systematic variability originating from the time-variable GCR flux. Ti signatures were used to estimate background signals following the procedures outlined by Evans et al. (2012) and Peplowski et al. (2012). The O signature was used to estimate the O-originating fraction of the 4438-keV peak.

3.2. Background reduction

The uncorrected 4438-keV gamma-ray count rate more than doubles as MESSENGER goes from high (>8000 km) to low (<2000 km) altitudes over Mercury's surface (Table 1), suggestive of a substantial planet-originating component. Prior to attributing this signal to C on Mercury's surface, important background corrections must be made (see Sections 2.3 and 2.4). The importance of these background signals is reinforced by the presence of a notable 4438-keV count rate (0.143 ± 0.005 counts min^{-1}) at high altitudes, as the high-altitude spectrum was acquired too far from Mercury to include a planet-originating component and thus requires a local source.

The high-altitude 4438-keV gamma-ray count rate originates from GCR-induced gamma-ray emission within the spacecraft. This background is inversely proportional to the altitude of the spacecraft as a result of obscuration of spacecraft-incident GCRs at low altitudes by the planet. This relationship is quantified via the solid angle (Ω), which is the altitude-dependent fraction of the 4π field of view that is subtended by Mercury. Ω is calculated as

$$\Omega(h) = \frac{1 - \cos\,\theta_{\max}(h)}{2} \quad (1)$$

where h is the orbital altitude and $\theta_{\max}$ is the angle between the sub-spacecraft nadir angle and the horizon. $\theta_{\max}$ is calculated from

$$\theta_{max}(h) = acos\left[\frac{[(R_M+h)^2 - R_M^2\,]^{1/2}}{(R_M+h)^2}\right] \quad (2)$$

where R_M is the radius of Mercury (2440 km). For the high-altitude spectrum, Ω is ≤ 0.01. This value contrasts with those for the low-altitude measurements, for which Ω ranges from 0.08 to 0.31 and has an average value of 0.15. The GCR-induced count rate, hereafter denoted $C_{GCR}(h)$, is proportional to the spacecraft-incident GCR flux and will decrease linearly with Ω as

$$C_{GCR}(h) = C_{GCR}^{HA}\left[1 - \Omega(h)\right] \quad (3)$$

where C_{GCR}^{HA} is the high-altitude ($\Omega \sim 0$) value. For the low-altitude measurements, $<\Omega> = 0.15$ and C_{GCR} is 0.121 ± 0.004 counts min^{-1}.

There is an additional background component that arises from the excitation of spacecraft material by Mercury originating neutrons. This background component increases as MESSENGER approaches Mercury with the same altitude dependence as the planet-originating signal of interest. Evans et al. (2012) estimated this contribution to the measured count rate through the "background amplification factor," a technique first developed by Rhodes et al. (2011). This technique utilizes the altitude-dependent increase in the 983-keV Ti peak as a proxy for all planetary-neutron-induced backgrounds. Ti was chosen because it is observed to have a strong signal in the gamma-ray spectra, despite the fact that its abundance on Mercury's surface as indicated by XRS measurements (Nittler et al., 2011) is well below the detection threshold for the GRS measurements. The Ti signal is attributed entirely to spacecraft backgrounds, most likely from the large amount of Ti within the walls of the spacecraft fuel tanks.

We adapt the background amplification factor (A) method of Evans et al. (2012), with minor modification. We define A as

$$A = \frac{C^{LA} - C_{GCR}^{LA}}{C^{HA}} \quad (4)$$

where C^{LA} and C^{HA} are the low- and high-altitude count rates, respectively, and C_{GCR}^{LA} is the GCR-component of the low-altitude (LA) signal (Eq. (3)). When used with an element for which the measured signal originates entirely from the spacecraft, A represents the background count rate induced by planetary neutrons relative to the GCR background count rate. This treatment is modified from that of Evans et al. (2012) in that we remove the GCR component of the LA count rate prior to calculating A. Evans et al. did not remove C_{GCR}^{LA}, but likewise they did not remove this component from C^{LA}, and as a result their A values contained both the GCR and planetary neutron background corrections. We consider our formalism to be more physically rigorous, although we note that the two procedures provide equivalent final results. Using the 983-keV Ti peak measurements (Table 1) and Eq. (3) to calculate C_{GCR}^{LA} for Ti, we obtain an A value of 0.65 ± 0.05. Like Evans et al. (2012), we assume that all backgrounds originating from interactions between planetary neutrons and spacecraft material scale identically with the Ti background. This assumption provides an estimate of the 4438-keV gamma-ray count rate resulting from Mercury originating neutrons hitting the spacecraft (C_{BG}) of

$$C_{BG} = C_{HA}A = (0.143 \pm 0.005)\ (0.65 \pm 0.05) = 0.093 \pm 0.004 \quad (5)$$

in units of counts min^{-1}.

Finally, we must remove the background component originating from 4438-keV gamma rays produced by ^{16}O(n,n$\alpha\gamma_{4438}$)^{12}C reactions in near-surface material on Mercury. We do this by scaling the measured 6129-keV O gamma-ray count rate by the ratio of 6129- to 4438-keV gamma rays expected on the basis of the ^{16}O(n,n$\alpha\gamma_{4438}$)^{12}C and ^{16}O(n,n$'\gamma_{4438}$)^{16}O cross section. The ratio, 0.41, is derived in the appendix (Eq. (A10)).

These estimated background signals allow us to calculate the contribution of O to the measured 4438-keV gamma-ray count rate. The procedure is as follows: (1) the planetary 6129-keV count rate is derived from the low-altitude 6129-keV peak area (Table 1) by removing the GCR component (Eq. (3)) and correcting for spacecraft excitation using A (Eq. (5)), the same as was done for the 4438-keV count rate; (2) the resulting rate is multiplied by (1–0.1) to remove the contribution from ^{16}O(n,p)^{16}N (note that ^{16}N beta decays to ^{16}O, followed by emission of a 6129-keV gamma ray 67% of the time); and (3) the residual value is multiplied by the ratio of 4438- to 6129-keV gamma-ray production from O (0.41; Eq. (A10)). The resulting value, 0.09 ± 0.01 counts min^{-1}, represents the contribution of O to the measured 4438-keV count rate.

4. Results

4.1. Carbon concentration

The portion of the low-altitude 4438-keV count rate originating from C in Mercury's surface can be calculated as summarized in Table 2 and detailed here. First, the low-altitude 4438-keV gamma-ray count rate (0.340 ± 0.025 counts min^{-1}; Table 1) is corrected for the GCR-induced background signal (0.121 ± 0.004 counts min^{-1}, Eq. (3)) and planet-originating neutron backgrounds (0.093 ± 0.004 counts min^{-1}, Eq. (5)). Next, the contribution from ^{16}O is removed (0.09 ± 0.01 counts min^{-1}, section 3.2) to reveal a residual count rate of 0.042 ± 0.028 counts min^{-1}. This value is ratioed to the 1779-keV Si gamma-ray count rate to yield a C/Si count rate ratio of 0.022 ± 0.015. Note that the planetary Si count rate was derived from the values in Table 1 and is corrected for a small GCR-induced background contribution following Eq. (5) as well as 1778-keV emissions from Al, which accounted for only 6% of the measured 1778-keV count rate.

Deriving a carbon concentration for Mercury's surface from our measured C/Si gamma-ray count rate ratio requires comparison

Please cite this article as: Peplowski, P.N., et al., Constraints on the abundance of carbon in near-surface materials on Mercury: Results from the MESSENGER Gamma-Ray Spectrometer. Planetary and Space Science (2015), http://dx.doi.org/10.1016/j.pss.2015.01.008

Table 2
Low-altitude signal components for the 4438-keV C gamma-ray signature.

Component	Description	Count rate (counts min^{-1})	Source
C_{GCR}	Background from GCR interactions with spacecraft	0.121 ± 0.004	Eq. (3)
C_{BG}	Background from planetary neutron interactions with spacecraft	0.093 ± 0.004	Eq. (5)
C_O [a]	Oxygen contribution to the measured planetary 4438-keV count rate	0.09 ± 0.01	[a]
C_P [b]	Residual, planet-originating 4438-keV C gamma-ray count rate	0.042 ± 0.028	[b]

[a] The planetary O count rate is derived from $C_{LA}(6129) - C_{GCR}(6129) - C_{BG}(6129)$ multiplied by $(1-0.1)$ to remove the fraction (0.1) of 6129-keV gamma rays originating from $^{16}O(n,n'\gamma)^{16}N$ reactions. This value, 0.22 ± 0.02 counts min^{-1}, is multiplied by the result of Eq. (A10) (0.39) to derive the 4438-keV count rate originating from $(n,n'\gamma)$ reactions on ^{16}O.

[b] This value is calculated from the low-altitude 4438-keV count rate (Table 1) by subtracting the C_{GCR}, C_{BG}, and C_O values.

with model rates derived from radiation transport simulations. Evans et al. (2012) presented details of the simulations used for the interpretation of MESSENGER GRS data. These simulations begin with an assumed Mercury surface composition that includes 50 ppm C and 24.6 wt% Si (Evans et al., 2012). This Si abundance is consistent with geochemical modeling of Mercury's surface composition (Stockstill-Cahill et al., 2012) and values derived from typical stoichiometry of major cations (Lawrence et al., 2013, Supplementary material). For the primary C (4438 keV) and Si (1779 keV) signatures, a C/Si gamma-ray count rate ratio of 6.69×10^{-5} was calculated from the model composition for our dataset. Linearly scaling this ratio to 1 wt% C (i.e., by a factor of 200) yields a C/Si count-rate ratio of 0.013.

Dividing our measured C/Si count rate ratio by the modeled ratio per wt% C yields a C abundance of 1.4 ± 0.9 wt% on Mercury's surface with the reference Si abundance of 24.6 wt%. A standard minimum detection threshold in nuclear and particle physics is that a signal should have a three-standard-deviation significance. Our result is within two standard deviations of 0 wt% C and therefore does not represent a statistically significant detection. Instead, we find an allowable C content of 0 to 4.1 wt% at the three-standard-deviation level.

4.2. Caveats

There are several limitations to our data reduction methodology. Included among them are systematic errors in the background corrections, specifically originating from gamma-ray production cross sections. Estimates of the uncertainties in these cross sections have typically ranged from 5 to 30% (e.g., Reedy, 1978; Kim et al., 2007). We have compared the interpolated gamma-ray production cross sections with recent laboratory measurements where possible (e.g., Nelson et al., 2001), and we found excellent agreement for the $^{12}C(n,n'\gamma)$ and $^{16}O(n,n'\gamma)$ cross sections. These results suggest that the gamma-ray production cross sections are more robust than is often stated. In either case, no effort to account for their uncertainties is included in our final uncertainties.

In addition, our use of the 6129-keV O gamma-ray line to estimate the ^{16}O contributions to the 4438-keV gamma ray may be problematic, as Evans et al. (2012) noted that the O abundance derived from this gamma ray is unrealistically (~20%) low. This result suggests that there may be some unidentified problem with the derivation of O abundances from measurements of the 6129-keV gamma-ray count rate. Although the impact of this issue on our background reduction procedure and final C abundance is unknown, we consider it unlikely that the error is in the derivation of the 6129-keV gamma-ray count rates measured by the GRS, the only input to our derivation of the C abundance. We therefore conclude that it is doubtful that the uncertainty with the O abundance affects our derived C abundance.

5. Discussion

5.1. Spatial distribution of C

The low counting rate of the C gamma-ray signature required summing all valid data acquired over Mercury's northern hemisphere prior to deriving a C concentration. As a result, the GRS measurements cannot directly provide any information regarding the distribution of any C that might be present on Mercury's surface. Fortunately, MESSENGER multispectral imaging can limit the possible scenarios. Murchie et al. (2015) invoked coarse (micrometer-sized) grains of graphite as a possible darkening agent for Mercury's surface. Through a combination of elemental abundance measurements and spectral modeling, they estimated that approximately 1 wt% graphite would be needed to produce the average northern hemisphere reflectance. They similarly found that up to 5 wt% could produce sufficient darkening to account for the measured reflectance of LRM. Note that the precise amounts of C needed to account for the observed darkening depend on the grain size of the graphite.

We used the spatial deconvolution techniques presented by Peplowski et al. (2014) to model the effective northern hemisphere concentration as observed by the GRS. Our inputs were Murchie et al. (2015) C concentration estimates (1 wt% global; 5 wt% in LRM), along with a global distribution of LRM derived with the identification criteria of Denevi et al. (2009). The resulting effective northern-hemisphere-averaged C content as seen by the GRS is 1.03 wt%. This value, which is almost identical to the global (non-LRM) value, highlights the fact that LRM is relatively scarce in the northern hemisphere, and that, despite its potentially higher C concentrations, the northern-hemisphere-averaged GRS result is not sensitive to the elemental composition of these units. As a consequence the GRS result does not address the possibility that C is driving the relative differences in reflectance among the spectral units on Mercury's surface.

5.2. Sources of C on Mercury

The GRS results allow for an average surface C abundance of 0 to 4.1 wt% C on Mercury. The possible existence of wt% concentrations of C on Mercury is surprising when compared with the low <1000 ppm average abundances of C in the crusts of Earth, the Moon, and Mars (Lodders and Fegley, 1998). A mechanism by which substantial amounts of C would have avoided sequestration into Mercury's core during differentiation has not been identified, although substantial amounts of S have been identified on the surface (Nittler et al., 2011; Evans et al., 2012) that likewise avoided incorporation into the core. The high abundance of S in the silicate portion of Mercury has been attributed to low oxygen fugacity (fO_2) values in the chemically reduced precursor materials from which Mercury was formed (Nittler et al., 2011; McCubbin et al., 2012; Stockstill-Cahill et al., 2012; Zolotov et al., 2013). Vander Kaaden and McCubbin (2015) noted that graphite is the only mineral to

Please cite this article as: Peplowski, P.N., et al., Constraints on the abundance of carbon in near-surface materials on Mercury: Results from the MESSENGER Gamma-Ray Spectrometer. Planetary and Space Science (2015), http://dx.doi.org/10.1016/j.pss.2015.01.008

remain buoyant with respect to melts of mercurian magmas, suggesting that any C that did escape sequestration into the core may have concentrated into a primary floatation crust during the cooling of a global magma ocean. The mechanisms for retaining C in Mercury's silicate portion are unknown, and the reducing conditions present in Mercury differ markedly from those that prevailed during the formation of Earth and the Moon. This difference complicates efforts to extrapolate current theories for geochemical processes occurring during terrestrial core formation to Mercury.

Enstatite chondrites may offer some insight into the presence of C on Mercury's surface. Nittler et al. (2011) noted that XRS-measured compositions for Mercury surface materials are reasonably well matched by the composition of silicate partial melts from the Indarch enstatite chondrite (McCoy et al., 1999). Enstatite chondrites are known to have relatively high C contents (0.06 to 0.6 wt%; Moore and Lewis, 1966), with the C frequently found as graphite (Keil, 1998). Inasmuch as partially melted enstatite chondrites are an analog for Mercury's surface composition, the highest C abundances of 0.6 wt% found by Moore and Lewis (1966) are at least broadly consistent with the possibility of ~1 wt% C on Mercury's surface as allowed by the GRS measurements (0–4.1 wt %). The silicate partial melt from Indarch has an Fe content of 0.09 to 0.44 wt% (McCoy et al., 1999), which when combined with the full range of bulk C abundances of Moore and Lewis (1966) yield Fe/C ratios of 0.7–7.1. The MESSENGER GRS C abundance value of 1.4 ± 0.9 wt% and the upper limit of 4.1 wt% can be combined with the corresponding GRS Fe abundance measurement for Mercury's northern hemisphere (1.9 ± 0.3 wt%; Evans et al., 2012) to yield Fe/C abundance ratios of 1.4 and 0.5, respectively. Note that this range of Fe/C ratios does not include the possibility of 0–1.3 wt% C, which is also allowed by the GRS measurement. Fe/C ratios of 1.4 and 0.5 are consistent with those for Indarch partial melt, which were calculated under the assumption that the C content of the silicate portion is similar to the bulk values for enstatite chondrites noted by Moore and Lewis (1966).

Another possible explanation for higher-than-expected abundances of C on Mercury's surface is exogenous delivery via meteoroid infall. Exogenous delivery of material is already suggested by a comparison of the measured Fe concentrations on Mercury's surface (1.9 wt% northern hemisphere average; Evans et al., 2012) to expectations (<0.6 wt%) inferred from geochemical modeling (Zolotov et al., 2013) and equilibrium metal-silicate melting experiments (Chabot et al., 2014). If a similar mechanism is invoked to emplace C on Mercury's surface, then the Fe/C values allowed by the GRS measurements may provide insight into the nature of the infalling material. A range of Fe/C values is allowed, from 0.3 to 1.4, depending on whether the GRS mean (1.4 wt% C) or maximum allowed (4.1 wt% C) is used, as well as whether 1.9 wt % Fe (measured) or 1.3 wt% Fe (derived exogenous component) is used. Note that this range of Fe/C ratios does not include the possibility of 0 to 1.3 wt% C, which is also allowed by the GRS measurement.

Our Fe/C ratios differ significantly from chondritic Fe/C abundance ratios (57–78; Lodders and Fegley, 1998) and indicate that ≥ 1.4 wt% abundances of C on Mercury's surface cannot originate solely from the gradual accumulation of chondritic meteoritic material. Even carbonaceous chondrites, for which Fe/C ratios can be as low as 5.3 (Lodders and Fegley, 1998), have insufficient C to account for a Fe/C ratio on Mercury of 0.3–1.4. If there is ≥ 1.4 wt% of exogenous C on Mercury's surface, then it must have been delivered by bodies with Fe/C ratios lower than even the most C-rich carbonaceous chondrites. Cometary impacts may provide an alternative delivery mechanism (e.g., Bruck Syal et al., 2013), and MESSENGER investigations of Mercury's polar deposits have provided evidence that such impacts have delivered carbon-bearing material to the surface (Neumann et al., 2013; Paige et al., 2013). However, any mechanism that invokes exogenous C delivery to explain Mercury's low reflectance, and particularly that of LRM, must account for the inferred stratigraphic position of the LRM deposits. These deposits are largely found in material that was exhumed by impacts (e.g., Fig. 1), and if attributed to exogenous delivery of C they imply a subsequent burial process.

6. C abundances from neutron spectroscopy

Fortunately, another avenue exists with which to investigate the possibility of C on Mercury's surface. MCNPX modeling of neutron emission from Mercury's surface indicates that 5 wt% C within the LRM would produce a notable change to Mercury's neutron flux (Fig. 5a). Specifically, increasing the C content of a typical Mercury regolith composition lowers the epithermal (0.2 eV to 0.5 MeV) neutron flux and raises the thermal (<2 eV) neutron flux (Fig. 5b). Other candidate elements that might cause the darkening (e.g., Fe, Ti) would result in a decrease in the thermal neutron flux (Elphic et al., 2000), the opposite behavior to that for the C signal. In addition, Fe and Ti are detectable with the XRS measurements, and to date there is no evidence that they have higher abundances in the LRM (Murchie et al., 2014). Whereas an increase in the thermal/fast neutron count rate accompanied by a decrease in the epithermal/fast neutron count rate over the LRM would not be an unambiguous signature for increased C, it would provide substantial support for higher C concentrations, particularly in the dry equatorial regions where hydrogen is not a plausible alternative. Hydrogen must be considered at higher latitudes because it, too, lowers the epithermal

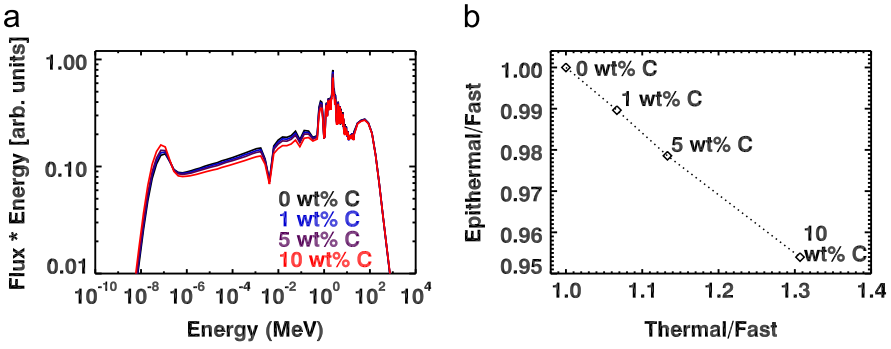

Fig. 5. (a) MCNPX-modeled neutron fluxes for Mercury calculated for a base composition similar to the intercrater plains and heavily cratered terrain (IcP-HCT) as measured by the MESSENGER XRS and GRS (Weider et al., 2012; Evans et al., 2012). 1, 5, and 10 wt% C were added to the IcP-HCT, and the resulting changes to the neutron flux were tracked. (b) The epithermal-to-fast neutron ratio plotted against the thermal-to-fast neutron ratio for the 0, 1, 5, and 10 wt% C MCNPX simulations. The figure shows that the epithermal neutron fluxes decrease with increasing C content and the thermal neutron fluxes increase with increasing C content.

Please cite this article as: Peplowski, P.N., et al., Constraints on the abundance of carbon in near-surface materials on Mercury: Results from the MESSENGER Gamma-Ray Spectrometer. Planetary and Space Science (2015), http://dx.doi.org/10.1016/j.pss.2015.01.008

neutron flux (more efficiently than does C), and for weight fractions $0.001 < H_2O < 0.1$ it can also raise the thermal neutron flux (Lawrence et al., 2006).

The challenges associated with measuring the C content of the LRM with the MESSENGER Neutron Spectrometer (NS) include the relative scarcity of this terrain and its small contiguous areas in the northern hemisphere. The largest LRM deposits in the northern hemisphere include the basin floor and ejecta deposits surrounding the inner peak ring of Rachmaninoff basin (Fig. 1) as well as two deposits (centered near 45° N, 305° E, and 35° N, 350° E) west of Derzhavin crater. Unlike the Rachmaninoff LRM deposit, the deposits west of Derzhavin are not directly correlated with impact features. Although these LRM deposits are the largest in the northern hemisphere, they are still smaller than the typical spatial resolution of the NS at mid-latitudes (FWHM ≥ 350 km). As a result, the 7% change in the thermal/fast neutron flux that would accompany a change in the C abundance from 1 to 5 wt% (Fig. 5b) would be reduced in proportion to the fraction of the NS footprint occupied by the LRM feature in view. Fortunately, low-altitude flyovers of these LRM deposits are planned during MESSENGER's final year of orbital operations. Because the spatial resolution of the NS measurements is proportional to the orbital altitude, the low-altitude orbits will provide the best opportunity to make spatially resolved measurements of LRM and constrain its possible C abundance. These measurements have the greatest potential to refute or support the hypothesis of large (~5 wt%) C abundances in the LRM.

7. Conclusions

Motivated by the suggestion that fine-grained graphite may be the dominant darkening agent on Mercury's surface (Murchie et al., 2015), we have used MESSENGER Gamma-Ray Spectrometer measurements of the 4438-keV C gamma-ray signature to derive a C abundance in Mercury surface material. This process required the application of background reduction techniques developed to remove spacecraft- and planet-originating backgrounds from the measurements. This procedure significantly increased the statistical uncertainty in the measurement. Our final result is an average northern hemisphere C abundance of 1.4 ± 0.9 wt% C, which corresponds to an allowable abundance range of 0–4.1 wt% at the three-standard-deviation significance level. Applying a three-standard-deviation discovery threshold, the minimum that should be considered, means that our measurement does not provide definitive identification of C on Mercury's surface. Fortunately, MESSENGER NS measurements will test the hypothesis of variable C abundances on Mercury's surface during the planned low-altitude campaign scheduled to occur in the final year of the mission.

The large uncertainty in our final result is primarily the result of the large background corrections that were applied to the 4438-keV count rate. Our general calculations of 4438-keV gamma-ray fluxes from C and O (Fig. 2) clearly show that, in the absence of large C backgrounds, gamma-ray spectroscopy is a promising technique for measuring C concentrations in excess of 0.5 wt% on planetary surfaces. The formalism presented here provides a framework for searching for C on other planetary surfaces with gamma-ray spectroscopy.

Acknowledgments

We thank the entire MESSENGER team for their invaluable contributions in the development and operation of the MESSENGER spacecraft. We also thank Robert Reedy for providing cross-section data and for engaging in enlightening conversations regarding their validity and application. Kathleen Vander Kaaden and Robert Reedy provided constructive comments on an earlier version of this paper. The MESSENGER mission is supported by the NASA Discovery Program under contract NAS5-97271 to The Johns Hopkins University Applied Physics Laboratory and NASW-00002 to the Carnegie Institution of Washington. LGE, DTB, and DJL acknowledge support from the MESSENGER Participating Scientist Program.

Appendix A. Calculation of gamma-ray fluxes from cross sections

The GCR-induced gamma-ray flux at the surface of a planet for a given element can be calculated with knowledge of the relevant gamma-ray production cross sections (σ_γ) and the GCR-induced neutron flux (N_n). The results of similar calculations have been previously reported (e.g., Reedy, 1978; Kim et al., 2007), but we present here a detailed formalism for these calculations because such descriptions are not typically provided in prior publications.

The gamma-ray flux at the surface of a planet (Φ_γ) for neutron-induced gamma-ray emission is a function of the reaction probability (σ_γ), the neutron flux (N_n), the number of atoms for the element of interest A_i, and the probability I that the gamma ray will reach the surface and escape with its full energy. Φ_γ is

$$\Phi_\gamma = \int_0^\infty \int_0^\infty \sigma_\gamma(E_n) N_n(E_n) I(E_\gamma, z) A_i(z) dE_n\, dz \quad \text{(A1)}$$

where E_n is the neutron energy, E_γ is the energy of the gamma ray emitted during the reaction of interest, and z is the depth beneath the surface at which the reaction occurs. Although both integrals extend from zero to infinity, in practice gamma-ray production drops off rapidly with energy and is negligible for $E_n > \sim 100$ MeV, and gamma-ray production for depths greater than many tens of centimeters is negligible. The following paragraphs describe each component of the integral in detail.

Reaction cross sections describe the probability that a nuclear reaction will occur. We utilize gamma-ray production cross sections (σ_γ), which describe the probability that a given reaction will occur and that it will result in the emission of a gamma ray at a particular energy. Fig. 2 illustrates the σ_γ values for 4438-keV gamma-ray production from the $^{12}C(n,n'\gamma)$ and $^{16}O(n,n'\alpha\gamma)$ reactions. The data originate from the evaluated cross sections of Kim et al. (2007). Cross sections are expressed in units of millibarns; one millibarn is equal to 10^{-27} cm^2.

The neutron flux, $N_n(E_n)$, is derived from MCNPX calculations (e.g., McKinney et al., 2006), which have been shown to successfully reproduce the GCR-induced neutron flux from Mercury to better than 10% (Lawrence et al., 2010). The neutron flux used in this work was calculated for an intercrater plains composition, as derived from the elemental composition measurements of Peplowski et al. (2011, 2012, 2014), Nittler et al. (2011), Evans et al. (2012, 2014), and Weider et al. (2012, 2014). Details of the neutron transport modeling are discussed in detail in the supplementary online material of Lawrence et al. (2013).

The fraction of gamma rays produced at a given depth z that reaches the surface at their full energy is calculated from

$$I(E_\gamma, d) = e^{-\rho a(E_\gamma) d(z,\theta)} \quad \text{(A2)}$$

where ρ is the density of the material at the surface (g/cm^3), $a(E_\gamma)$ is the attenuation coefficient (cm^2/g) as derived from the NIST XCOM database (Berger et al., 1987), and d the distance between the gamma-ray production site and the surface (cm), which depends on both the depth of the production site (z) and the

Please cite this article as: Peplowski, P.N., et al., Constraints on the abundance of carbon in near-surface materials on Mercury: Results from the MESSENGER Gamma-Ray Spectrometer. Planetary and Space Science (2015), http://dx.doi.org/10.1016/j.pss.2015.01.008

emission angle (θ) as

$$d = \frac{z}{\cos\ \theta} \tag{A3}$$

In Eq. (A1), $A_i(z)$ describes the atomic density for the element of interest in units of cm^{-3}, which can in principle be depth (z) dependent, but can be assumed to be constant for a well-mixed regolith, such as that expected for the top tens of centimeters of Mercury's regolith. For the purpose of this analysis, we remove the z dependence and define A_i as

$$A_i = \chi_i A_{tot} \tag{A4}$$

where χ_i is the molar fraction for the element of interest (i) and A_{tot} is the atomic density of the soil and includes all constituents.

The expression for the gamma-ray flux at the surface can be simplified by removing the atomic density from the integrals and evaluating them separately as

$$\Phi_\gamma = \chi_i A_{tot} \int_0^{100\ MeV} \sigma_\gamma(E_n) N_n(E_n) dE_n \int_0^{1\ m} I(E_\gamma, z) dz \tag{A5}$$

Solving for gamma-ray production ratios can be further simplified. For example, the relative production of 4438-keV gamma rays (γ_{4438}) from C and O is calculated as

$$R = \frac{\Phi^{Carbon}_{\gamma_{4438}}}{\Phi^{Oxygen}_{\gamma_{4438}}} = \frac{\chi_{Carbon} \int_0^{100\ MeV} \sigma_{^{12}C(n,n'\gamma_{4438})}(E_n) N_n(E_n) dE_n}{\chi_{Oxygen} \int_0^{100\ MeV} \sigma_{^{16}O(n,n'\alpha\gamma_{4438})}(E_n) N_n(E_n) dE_n} \tag{A6}$$

where the integral over z cancels since the gamma rays have identical energy and by extension identical attenuation probabilities in the regolith. This ratio reduces to

$$R = \frac{\chi_{Carbon}}{\chi_{Oxygen}} 5.9 \tag{A7}$$

and this expression was used to derive the results shown in Fig. 2 (inset).

Where the z integrals do not cancel, they can be solved to derive attenuation ratios. For example, the background reduction calculations of Section 3.2 required knowledge of attenuation of 6129-keV gamma rays relative to 4438-keV gamma rays. The ratio of the integrals

$$\frac{\int_0^{1\ m} I(E_\gamma = 6129\ keV,\ z) dz}{\int_0^{1\ m} I(E_\gamma = 4438\ keV,\ z) dz} = 0.95 \tag{A8}$$

provides the correction factor to account for the higher attenuation of 4438-keV gamma rays within the regolith relative to 6129-keV gamma rays. This step facilitates solving for the ratio of 4438- to 6129-keV gamma-ray production from O as

$$R = \frac{\Phi^{Oxygen}_{\gamma_{4438}}}{\Phi^{Oxygen}_{\gamma_{6129}}} = 0.95 \frac{\int_0^{100\ MeV} \sigma_{^{16}O(n,n'\alpha\gamma_{4438})}(E_n) N_n(E_n) dE_n}{\int_0^{100\ MeV} \sigma_{^{16}O(n,n'\gamma_{6129})}(E_n) N_n(E_n) dE_n} = 0.26 \tag{A9}$$

Note that the ratio of the abundance has canceled out, and the relative attenuation of the two gamma rays in Eq. (A8) has been included. Finally, our measured ratio (R_{meas}) also depends on the detection efficiency for 4438-keV gamma rays, $\varepsilon(4438)$, relative to that of the 6129-keV gamma rays, $\varepsilon(6129)$, taken from Peplowski et al. (2012), as

$$R_{meas} = R \frac{\varepsilon(4438)}{\varepsilon(6129)} = 0.26 \frac{0.030}{0.019} = 0.41 \tag{A10}$$

As a test of the validity of this formalism, we calculated the gamma-ray flux ratios for S/Si (2231-keV S and 1779-keV Si), Ca/Si (3737-keV Ca), and Fe/Si (846-keV Fe) for Mercury and compared them with the measured count-rate ratios of Evans et al. (2012). All agreed to within 20%, validating the use of this formalism to calculate first-order gamma-ray fluxes without the use of full-planet gamma-ray production modeling.

References

Berger, M.J., Hubbell, J.H., Seltzer, S.M., Chang, J., Coursey, J.S., Sukumar, R., Zucker, D.S., Olsen, K., 1987. XCOM: Photon Cross Sections on a Personal Computer (Report NBSIR 87-3597). National Institute of Standards and Technology, Gaithersburg, Maryland.

Blewett, D.T., Robinson, M.S., Denevi, B.W., Gillis-Davis, J.J., Head, J.W., Solomon, S.C., Holsclaw, G.M., McClintock, W.E., 2009. Multispectral images of Mercury from the first MESSENGER flyby: analysis of global and regional color trends. Earth Planet. Sci. Lett. 285, 227–282. http://dx.doi.org/10.1016/j.epsl.2009.02.021.

Boynton, W.V., Taylor, J.G., Evans, L.G., Reedy, R.C., Starr, R., Janes, D.M., Kerry, K.E., Drake, D.M., Kim, K.J., Williams, R.M.S., Crombie, M.K., Dohm, J.M., Baker, V., Metzger, A.E., Karunatillake, S., Keller, J.M., Newsom, H.E., Arnold, J.R., Brückner, J., Englert, P.A.J., Gasnault, O., Sprague, A.L., Mitrofanov, I., Squyres, S.W., Trombka, J.I., d'Uston, L., Wänke, H., Hamara, D.K., 2007. Concentration of H, Si, Cl, K, Fe, and Th in the low- and mid-latitude regions of Mars. J. Geophys. Res. 112, E12S99. http://dx.doi.org/10.1029/2007JE002887.

Braden, S.E., Robinson, M.S., 2013. Relative rates of optical maturation of regolith on Mercury and the Moon. J. Geophys. Res. Planets 118, 1903–1914. http://dx.doi.org/10.1002/jgre.20143.

BruckSyal, M., Schultz, P.H., Riner, M.A., 2013. Painting Mercury by comet-delivered carbon. Lunar Planet. Sci. 44 (abstract 2496).

Chabot, N.L., Wollack, E.A., Klima, R.L., Minitti, M.E., 2014. Experimental constraints on Mercury's core composition. Earth. Planet. Sci. Lett. 390, 199–208. http://dx.doi.org/10.1016/j.epsl.2014.01.004.

Denevi, B.W., Robinson, M.S., Solomon, S.C., Murchie, S.L., Blewett, D.T., Domingue, D.L., McCoy, T.J., Ernst, C.M., Head, J.W., Watters, T.R., Chabot, N.L., 2009. The evolution of Mercury's crust: a global perspective from MESSENGER. Science 324, 613–618. http://dx.doi.org/10.1126/science.1172226.

Elphic, R.C., Lawrence, D.J., Feldman, W.C., Barraclough, B.L., Maurice, S., Binder, A.B., Lucey, P.G., 2000. Lunar rare earth element distribution and ramifications for FeO and TiO_2: Lunar Prospector neutron spectrometer observations. J. Geophys. Res. 105, 20,333–20,345. http://dx.doi.org/10.1029/1999JE001176.

Ernst, C.M., Murchie, S.L., Barnouin, O.S., Robinson, M.L., Denevi, B.W., Blewett, D.T., Head, J.W., Izenberg, N.R., Solomon, S.C., Roberts, J.H., 2010. Exposure of spectrally distinct material by impact craters on Mercury: implications for global stratigraphy. Icarus 209, 210–223. http://dx.doi.org/10.1016/j.icarus.2010.05.022.

Evans, L.G., Reedy, R.C., Starr, R.D., Kerry, K.E., Boynton, W.V., 2006. Analysis of gamma ray spectra measured by Mars Odyssey. J. Geophys. Res. 111, E03S04. http://dx.doi.org/10.1029/2005JE002657.

Evans, L.G., Peplowski, P.N., Rhodes, E.A., Lawrence, D.J., Nittler, L.R., McCoy, T.J., Solomon, S.C., Sprague, A.L., Stockstill-Cahill, K.R., Starr, R.D., Weider, S.Z., Boynton, W.V., Hamara, D.K., 2012. Major-element abundances on the surface of Mercury: results from the MESSENGER Gamma-Ray Spectrometer. J. Geophys. Res. 117, E00L07. http://dx.doi.org/10.1029/2012JE004178.

Evans, L.G., Peplowski, P.N., Ebel, D.S., Lawrence, D.J., McCoy, T.J., Nittler, L.R., Starr, R.D., Weider, S.Z., Solomon, S.C., 2014. Chlorine on the surface of Mercury: implications for Mercury's surface evolution. In: Proceedings of the Lunar and Planetary Science Conference, 45, 1794, abstract.

Goldsten, J.O., Rhodes, E.A., Boynton, W.V., Feldman, W.C., Lawrence, D.J., Trombka, J.I., Smith, D.M., Evans, L.G., White, J., Madden, N.W., Berg, P.C., Murphy, G.A., Gurnee, R.S., Strohbehn, K., Williams, B.D., Schaefer, E.D., Monaco, C.A., Cork, C.P., Eckels, J.D., Miller, W.O., Burks, M.T., Hagler, L.B., DeTeresa, S.J., Witte, M.C., 2007. The MESSENGER Gamma-Ray and Neutron Spectrometer. Space Sci. Rev. 131, 339–391. http://dx.doi.org/10.1007/s11214-007-9262-7.

Keil, K., 1998. Enstatite meteorites and their parent bodies. Meteoritics 24, 195–208. http://dx.doi.org/10.111/j.1945-5100.1989.tb00649.x.

Kim, K.J., Drake, D.M., Reedy, R.C., Williams, R.M.S., Boynton, W.V., 2007. Theoretical fluxes of gamma rays from the Martian surface. J. Geophys. Res. 111, E03S09. http://dx.doi.org/10.1029/2005JE002655.

Lawrence, D.J., Feldman, W.C., Elphic, R.C., Hagerty, J.J., Maurice, S., McKinney, G.W., Prettyman, T.H., 2006. Improved modeling of Lunar Prospector Neutron Spectrometer data: implications for hydrogen deposits at the lunar poles. J. Geophys. Res. 111, E08001. http://dx.doi.org/10.1029/2005JE002637.

Lawrence, D.J., Feldman, W.C., Goldsten, J.O., McCoy, T.J., Blewett, D.T., Boynton, W.V., Evans, L.G., Nittler, L.R., Rhodes, E.A., Solomon, S.C., 2010. Identification and measurement of neutron-absorbing elements on Mercury's surface. Icarus 209, 195–209. http://dx.doi.org/10.1016/j.icarus.2010.04.005.

Lawrence, D.J., Feldman, W.C., Goldsten, J.O., Maurice, S., Peplowski, P.N., Anderson, B.J., Bazell, D., McNutt Jr., R.L., Nittler, L.R., Prettyman, T.H., Rodgers, D.J., Solomon, S.C., Weider, S.Z., 2013. Evidence for water ice near Mercury's north pole from MESSENGER neutron spectrometer measurements. Science 339, 292–296. http://dx.doi.org/10.1126/science.1229953.

Lodders, K., Fegley Jr., B., 1998. The Planetary Scientist's Companion. Oxford University Press, New York.

Lucey, P.G., Riner, M.A., 2011. The optical effects of small iron particles that darken but do not redden: evidence for intense space weathering on Mercury. Icarus 212, 451–462. http://dx.doi.org/10.1016/j.icarus.2011.01.002.

McCoy, T.J., Dickinson, T.L., Lofgren, G.E., 1999. Partial melting of the Indarch (EH4) meteorite: a textural, chemical, and phase relations view of melting and melt migration. Meteorit. Planet. Sci. 34, 734–746. http://dx.doi.org/10.1111/j.1945-5100.1999.tb01386.x.

McCubbin, F.M., Riner, M.A., Vander Kaaden, K.E., Burkemper, L.K., 2012. Is Mercury a volatile-rich planet? Geophys. Res. Lett. 39, L09292. http://dx.doi.org/10.1029/2012GL051711.

Please cite this article as: Peplowski, P.N., et al., Constraints on the abundance of carbon in near-surface materials on Mercury: Results from the MESSENGER Gamma-Ray Spectrometer. Planetary and Space Science (2015), http://dx.doi.org/10.1016/j.pss.2015.01.008

McKinney, G.W., Lawrence, D.J., Prettyman, T.H., Elphic, R.C., Feldman, W.C., Hagerty, J.J., 2006. MCNPX benchmark for cosmic ray interactions with the Moon. J. Geophys. Res. 111, E06004. http://dx.doi.org/10.1029/2005JE002551.

Moore, C.B., Lewis, C.F., 1966. The distribution of total carbon content in enstatite chondrites. Earth Planet. Sci. Lett. 1, 376–378.

Murchie, S.L., Klima, R.L., Denevi, B.W., Ernst, C.M., Keller, M.R., Domingue, D.L., Blewett, D.T., Chabot, N.L., Hash, C.D., Malaret, E., Izenberg, N.R., Vilas, F., Nittler, L.R., Gillis-Davis, J.J., Head, J.W., 2015. Orbital multispectral mapping of Mercury by MESSENGER: evidence for the origins of plains units and low-reflectance material. Lunar Planet. Sci. 46 (abstract 1606).

Nelson, R.O., Chadwick, M.B., Michaudon, A., Young, P.G., 2001. High-resolution measurements and calculations of photon-production cross sections for $^{16}O(n, x\gamma)$ reactions induced by neutrons with energies between 4 and 200 MeV. Nucl. Sci. Eng. 138, 105–144.

Neumann, G.A., Cavanaugh, J.F., Sun, X., Mazarico, E.M., Smith, D.E., Zuber, M.T., Mao, D., Paige, D.A., Solomon, S.C., Ernst, C.M., Barnouin, O.S., 2013. Bright and dark polar deposits on Mercury: evidence for surface volatiles. Science 339, 296–300. http://dx.doi.org/10.1126/science.1229764.

Nittler, L.R., Starr, R.D., Weider, S.Z., McCoy, T.J., Boynton, W.V., Ebel, D.S., Ernst, C.M., Evans, L.G., Goldsten, J.O., Hamara, D.K., Lawrence, D.J., McNutt Jr., R.L., Schlemm II, C.E., Solomon, S.C., Sprague, A.L., 2011. The major element composition of Mercury's surface from MESSENGER X-ray spectrometry. Science 333, 1847–1850. http://dx.doi.org/10.1126/science.1211567.

Noble, S.K., Pieters, C.M., 2003. Space weathering on Mercury: implications for remote sensing. Sol. Syst. Res. 37, 31–35. http://dx.doi.org/10.1023/A:1022395605024.

Paige, D.A., Siegler, M.A., Harmon, J.K., Neumann, G.A., Mazarico, E.M., Smith, D.E., Zuber, M.T., Harju, E., Delitsky, M.L., Solomon, S.C., 2013. Thermal stability of volatiles in the north polar region of Mercury. Science 339, 300–303. http://dx.doi.org/10.1126/science.1231106.

Pelowitz, D.B. (Ed.), 2005. MCNPX User's Manual. Los Alamos National Laboratory, Los Alamos, New Mexico (Version 2.5.0. Report LA-UR-94-1817).

Peplowski, P.N., Evans, L.G., Hauck II, S.A., McCoy, T.J., Boynton, W.V., Gillis-Davis, J.J., Ebel, D.S., Goldsten, J.O., Hamara, D.K., Lawrence, D.J., McNutt Jr., R.L., Nittler, L.R., Solomon, S.C., Rhodes, E.A., Sprague, A.L., Starr, R.D., Stockstill-Cahill, K.R., 2011. Radioactive elements on Mercury's surface from MESSENGER: implications for the planet's formation and evolution. Science 333, 1850–1853. http://dx.doi.org/10.1126/science.1211576.

Peplowski, P.N., Lawrence, D.J., Rhodes, E.A., Sprague, A.L., McCoy, T.J., Denevi, B.W., Evans, L.G., Head, J.W., Nittler, L.R., Solomon, S.C., Stockstill-Cahill, K.R., Weider, S.Z., 2012. Variations in the abundances of potassium and thorium on the surface of Mercury: results from the MESSENGER Gamma-Ray Spectrometer. J. Geophys. Res. 117, E00L04. http://dx.doi.org/10.1029/2012JE004141.

Peplowski, P.N., Evans, L.G., Stockstill-Cahill, K.R., Lawrence, D.J., McCoy, T.J., Nittler, L.R., Solomon, S.C., Sprague, A.L., Starr, R.D., Weider, S.Z., 2014. Enhanced sodium abundance in Mercury's north polar region revealed by the MESSENGER Gamma-Ray Spectrometer. Icarus 228, 86–95. http://dx.doi.org/10.1016/j.icarus.2013.09.007.

Prettyman, T.H., Haggerty, J.J., Elphic, R.C., Feldman, W.C., Lawrence, D.J., McKinney, G.W., Vaniman, D.T., 2006. Elemental composition of the lunar surface: analysis of gamma ray spectroscopy data from Lunar Prospector. J. Geophys. Res. 111, E12007. http://dx.doi.org/10.1029/2005JE002656.

Prettyman, T.H., Mittlefehldt, D.W., Yamashita, N., Lawrence, D.J., Beck, A.W., Feldman, W.C., McCoy, T.J., McSween, H.Y., Toplis, M.J., Titus, T.N., Tricarico, P., Reedy, R.C., Hendricks, J.S., Forni, O., Le Corre, L., Li, J.-Y., Mizzon, H., Reddy, V., Raymond, C.A., Russell, C.T., 2012. Elemental mapping by Dawn reveals exogenic H in Vesta's regolith. Science 338, 242–246. http://dx.doi.org/10.1126/science.1225354.

Prockter, L.M., Ernst, C.M., Denevi, B.W., Chapman, C.R., Head III, J.W., Fassett, C.I., Merline, W.J., Solomon, S.C., Watters, T.R., Strom, R.G., Cremonese, G., Marchi, S., Massironi, M., 2010. Evidence for young volcanism on Mercury from the third MESSENGER flyby. Science 329, 668–671. http://dx.doi.org/10.1126/science.1188186.

Reedy, R.C., 1978. Planetary gamma-ray spectroscopy. In: Proceedings of the 9th Lunar and Planetary Science Conference, pp. 2961–2984.

Rhodes, E.A., Evans, L.G., Nittler, L.R., Starr, R.D., Sprague, A.L., Lawrence, D.J., McCoy, T.J., Stockstill-Cahill, K.R., Goldsten, J.O., Peplowski, P.N., Hamara, D.K., Boynton, W.V., Solomon, S.C., 2011. Analysis of MESSENGER Gamma-Ray Spectrometer data from the Mercury flybys. Planet. Space Sci. 59, 1820–1841. http://dx.doi.org/10.1016/j.pss.2011.07.018.

Riner, M.A., Lucey, P.G., Desch, S.J., McCubbin, F.M., 2009. Nature of opaque components on Mercury: insights into a Mercurian magma ocean. Geophys. Res. Lett. 36, L02201. http://dx.doi.org/10.1029/2008GL036128.

Robinson, M.S., Murchie, S.L., Blewett, D.T., Domingue, D.L., Hawkins III, S.E., Head, J.W., Holsclaw, G.M., McClintock, W.E., McCoy, T.J., McNutt Jr., R.L., Prockter, L.M., Solomon, S.C., Watters, T.R., 2008. Reflectance and color variations on Mercury: regolith processes and compositional heterogeneity. Science 321, 66–69. http://dx.doi.org/10.1126/science.1160080.

Schlemm II, C.E., Starr, R.D., Ho, G.C., Bechtold, K.E., Hamilton, S.A., Boldt, J.D., Boynton, W.V., Bradley, W., Fraeman, M.E., Gold, R.E., Goldsten, J.O., Hayes, J.R., Jaskulek, S.E., Rossano, E., Rumpf, R.A., Schaefer, E.D., Strohbehn, K., Shelton, R.G., Thompson, R.E., Trombka, J.I., Williams, B.D., 2007. The X-Ray Spectrometer on the MESSENGER spacecraft. Space Sci. Rev. 131, 393–415. http://dx.doi.org/10.1007/s11214-007-9248-5.

Stockstill-Cahill, K.R., McCoy, T.J., Nittler, L.R., Weider, S.Z., Hauck II, S.A., 2012. Magnesium-rich crustal compositions on Mercury: implications for magmatism from petrologic modeling. J. Geophys. Res. 117, E00L15. http://dx.doi.org/10.1029/2012JE004140.

Vander Kaaden, K.E., McCubbin, F.M., 2015. Exotic crust formation on Mercury: consequences of a shallow, FeO-poor mantle. J. Geophys. Res. http://dx.doi.org/10.1002/2014JE004733, in press.

Weider, S.Z., Nittler, L.R., Starr, R.D., Byrne, P.K., Denevi, B.W., Solomon, S.C., 2012. Chemical heterogeneity on Mercury's surface revealed by the MESSENGER X-Ray Spectrometer. J. Geophys. Res. 117, E00L05. http://dx.doi.org/10.1029/2012JE004153.

Weider, S.Z., Nittler, L.R., Starr, R.D., McCoy, T.J., Solomon, S.C., 2014. Variations in the abundance of iron on Mercury's surface from MESSENGER X-Ray Spectrometer observations. Icarus 235, 170–186.

Zolotov, M.Yu., Sprague, A.L., Hauck II, S.A., Nittler, L.R., Solomon, S.C., Weider, S.Z., 2013. The redox state, FeO content, and origin of sulfur-rich magmas on Mercury. J. Geophys. Res. Planets 118, 138–146. http://dx.doi.org/10.1029/2012JE004274.

Please cite this article as: Peplowski, P.N., et al., Constraints on the abundance of carbon in near-surface materials on Mercury: Results from the MESSENGER Gamma-Ray Spectrometer. Planetary and Space Science (2015), http://dx.doi.org/10.1016/j.pss.2015.01.008